Helicase-Like Functions in Phosphate Loop Containing Beta-Alpha Polypeptides

Pratik Vyas[1], Olena Trofimyuk[1], Liam M. Longo[2], Fanindra Kumar Deshmukh[1], Michal Sharon[1] and Dan S. Tawfik[1]*

[1]Department of Biomolecular Sciences, Weizmann Institute of Science, Rehovot, Israel

[2]Tokyo Institute of Technology, Earth-Life Science Institute, Tokyo, Japan and Blue Marble Space Institute of Science

*Corresponding author. **E-mail:** dan.tawfik@weizmann.ac.il

Abstract

The P-loop Walker A motif underlies hundreds of essential enzyme families that bind NTPs and mediate phosphoryl transfer (P-loop NTPases), including the earliest DNA/RNA helicases, translocases and recombinases. What were the primordial precursors of these enzymes? Could these large and complex proteins emerge from simple polypeptides? Previously, we showed that P-loops embedded in simple βα repeat proteins bind NTPs, but also, unexpectedly so, ssDNA and RNA. Here, we extend beyond the purely biophysical function of ligand binding to demonstrate rudimentary helicase-like activities. We further constructed simple 40-residue polypeptides comprising just one β-(P-loop)-α motif. Despite their simplicity, these P-loop prototypes confer functions such as strand separation and exchange. Foremost, these polypeptides unwind dsDNA, and upon addition of NTPs, or inorganic polyphosphates, release the bound ssDNA strands to allow reformation of dsDNA. Binding kinetics and low-resolution structural analyses indicate that activity is mediated by oligomeric forms spanning from dimers to high-order assemblies. These tantalizing resemblances to extant P-loop helicases and recombinases suggest that these engineered P-loop prototypes comprise a plausible description of the sequence, structure and function of the earliest P-loop NTPases. These prototypes also indicate that multifunctionality and dynamic assembly were key in endowing short polypeptides with elaborate, evolutionarily relevant functions.

Introduction

Protein machines, such as ATP synthetases, helicases or RecA recombinases, perform remarkable actions and are immensely complex [1,2]. Among other factors, complexity is manifested in the concerted action of multiple functional elements, the proper alignment of which demands large, well-defined structures. This complexity is, however, at odds with the assumption that proteins emerged by duplication and fusion of relatively small and simple polypeptides [3,4]. Such polypeptides have two key limitations: they cannot afford the structural volume and complexity of intact domains, and they can in principle carry only one functional element. Further, these polypeptides predated the last universal common ancestor (LUCA) and as such cannot be reconstructed by conventional phylogenetic methods. However, despite nearly 4 BY of evolution, and extensive diversification of sequence, structure and function, these ancestral polypeptides are traceable by virtue of being the most conserved and functionally essential motifs of modern-day proteins [5]. Perhaps the most widely spread motif is the Walker-A P-loop [6]. Defined as GxxxxGK(T/S) or GxxGxGK, this motif underlies the most abundant and diverse protein class: the P-loop NTPases [6–9]. Structurally, the P-loop NTPase domain comprises a tandem repeat of at least five β-(loop)-α elements arranged in a αβα 3-layer sandwich architecture [7,8,10]. The loops connecting the C-termini of the β-strands to the N-termini of the following α-helices comprise the active site, while short loops link the β-(loop)-α elements to one another (here, unless stated otherwise, loops refer to the former). The Walker A P-loop is the key element mediating NTP binding and catalysis, and it uniformly resides within the first β-(loop)-α element, henceforth designated as β1-(P-loop)-α1.

P-loop NTPases are among the most ancient enzyme families – if not the most ancient enzyme family itself – and likely emerged at the transition from the RNA world to the primordial RNA-protein world [5,11–13]. Binding of phospho-ligands, foremost ATP and GTP, is the founding function of P-loop NTPases, as indicated by our previous analysis [14]. Indeed, the key to phospho-ligand binding is not only the P-loop, but also a 'crown' of hydrogen bonds realized by the end of the Walker A motif (GK(T/S) that comprises the first turn of α1 (Refs. [14,15]). It has been accordingly hypothesized that polypeptides comprising the P-loop and its flanking secondary structural elements, namely, a β-(P-loop)-α segment, were the seed from which modern P-loop NTPases emerged [5,16–18].

Previously, we showed that an ancestral β1-(P-loop)-α1 motif, inferred via phylogenetic analysis of all known P-loop NTPase families, could be grafted onto a simple repeat scaffold comprised of four consecutive βα elements [16]. This grafting resulted in simple proteins that contained two P-loops. These proteins bound ATP and GTP, but also, rather unexpectedly, RNA and ssDNA, via

the P-loop motif. It is therefore likely that the primordial P-loop was a multifunctional, generalist phospho-ligand binder that could function in the absence of other auxiliary residues [16]. In the contemporary P-loop NTPases, ssDNA binding is mostly conferred by specialized domains [19–22] distinct from the ATP binding P-loop [23]. And yet, in support of the P-loop's multifunctionality, we searched for and revealed examples of ssDNA binding mediated by the Walker A P-loop (detailed in 'Discussion'). Further, many of the P-loop NTPases families that date back to LUCA are involved in RNA/DNA remodeling, including helicases, such as Rec-A like recombinases and translocases [24]. ATP synthetase, for example, is thought to have emerged from these nucleic acid-remodeling P-loop NTPases [25].

That ssDNA binding can be mediated by the P-loop in our prototypes as well as in contemporary helicases, and the possible origins of P-loop NTPases as nucleic acid remodelers, guided us to extend our previous study [16] beyond the realm of ligand binding *per se*. We now (*i*) examine the potential of P-loop prototypes to exert, biological and evolutionarily relevant, helicase-like functions, *i.e.*, to mediate unwinding or strand separation of dsDNA and (*ii*) identify the minimal structural context in which the P-loop can confer these relevant functions.

Results

P-loop prototypes mediate strand separation

dsDNA undergoes spontaneous local fluctuations referred to as "DNA breathing," [26,27] thus giving access to ssDNA binding proteins [28]. For instance, T4 helicases bind to and stabilize these transient open regions to unwind dsDNA [27] — a mode of unwinding also referred to as "passive unwinding" [29]. To test the potential of P-loop prototypes to facilitate strand-separation, we used a standard fluorescence-based helicase assay dubbed a molecular beacon [30] (**Figure 1A**). This assay uses a dsDNA segment comprised of a "beacon oligo" with a fluorophore at the 5' end and a quencher at the 3' end (the sense strand) hybridized to an "unlabeled" complementary antisense-strand (**Supplementary Table S1**). Upon addition of a protein that promotes strand separation, owing to its complementary ends, the beacon strand collapses into an intramolecular hairpin. This brings together the fluorophore and the quencher, thus quenching the beacon's fluorescent signal.

For the initial round of experiments, the originally described 110 amino acid protein that presents two P-loops, hereafter referred to as the 'intact prototype', was used (D-Ploop [16]). When added to the beacon dsDNA, the intact prototype induced strand separation as indicated by the decrease in fluorescence (**Figure 1B**). The P-loop prototype showed negligible quenching of the fluorophore itself, as indicated by a negligible change in fluorescence intensity upon addition to digested beacon dsDNA (**Figure 1B**). Nonetheless, this non-specific quenching was subtracted

prior to analysis of the quenching traces reported later (see Methods). As elaborated below, strand-separation induced by the intact prototype occurred in two phases: an initial fast phase followed by a second slow phase (**Figure 1B**). Strand-separation, as reported by this beacon dsDNA, was the preliminary test for function of fragments of the intact P-loop prototype, as described in the next section.

Structural minimization of the P-loop prototype

The intact P-loop prototypes were based on an 'ideal fold' [31] that reproduces the 3-layered αβα sandwich architecture [7,8,10,24]. They are composed of four βα elements with the ancestral β-(P-loop)-α element replacing the first and third elements [16]. We asked whether the intact prototype could be truncated while retaining, or possibly even augmenting its function. In other words, what is the minimal 'stand-alone' P-loop fragment that possesses phospho-ligand binding and strand-separation activity?

The repeat nature of our prototypes allowed multiple options for the single P-loop constructs with varied structural topologies. In the first step, following our original report, the first half of the intact P-loop prototype (N-half) was tested [16]. Other 'half' constructs comprising two strands and two helices were also tested (**Figure 1C**, **Supplementary Figure S1**). Secondly, we used circular permutation to generate half fragments that possessed a αβαβ architecture (**Figure 1C**). All of these constructs, and especially the circular permutants, showed high expression and purification yields (via a His-tag and Ni-NTA; **Supplementary Figure S2A**). However, to maintain solubility at high protein concentrations, an osmolyte such as L-arginine was needed. We then truncated the circularly permuted 'half' constructs further to obtain the minimal constructs described below (**Figure 1C, Supplementary Figure S1**).

All 'half' constructs, and most of their truncated versions, mediated strand-separation to some degree (**Supplementary Figure S2B**). However, nucleic acid binding is known to be highly sensitive to ionic strength, and indeed the activity of most constructs was diminished in the presence of 100 mM NaCl. (**Figure 1D, Supplementary figure S2C**). We therefore set our assay conditions at 100 mM NaCl as a benchmark for robust activity. Intriguingly, under this stringent binding condition, a truncated variant dubbed 'N-αβα', comprising the ancestral β-(P-loop)-α element with one additional helix that precedes it, showed the most efficient and rapid strand separation (red trace; **Figure 1D**). Also worth noting is that 'N-αβα (and other P-loop prototypes) possesses low sequence complexity – it is made of only 12 amino acid types, 10 of which are considered abiotic, plus two basic amino acids, Lys and Arg (excluding the a 6xHistag for purification, and a tryptophan introduced for determining concentration by absorbance at 280 nm; **Table S2B**).

The minimal P-loop fragment

Can the N-αβα construct be further shortened? Three truncation constructs were generated by truncating the N-terminal helix to varying degrees. Given its polar nature, the primary role of this helix might be to enhance protein solubility (**Figure 1C, steps 4-6, Supplementary Table S2B**). Partial truncations of the N-terminal helix showed very similar activity to the intact N-αβα (N-αβα short_2 (green) trace; **Figure 1D**), while its complete truncation resulted in loss of the strand-separation activity (βα (blue) trace, **Figure 1D**). Nonetheless, this shortest construct, which in effect comprises a β-(P-loop)-α fragment, tended to co-purify with nucleic acids, suggesting that it retained some binding capability. The functional prototype N-αβα short_2 contains only a short N-terminal segment (KRRGV) linked to the β-(P-loop)-α fragment by a short linker (GSG; **Supplementary table S2B**). It therefore appears that given a charged leading segment, a single β-(P-loop)-α fragment can confer strand-separation activity.

The strand-separation activity is correlated with preferred binding of the P-loop prototypes to ssDNA over dsDNA, as indicated by ELISA experiments (**Figure 1E**; also observed for the intact P-loop prototypes reported in our previous study, by both ELISA and surface plasmon resonance [16]). These results suggest that the P-loop prototypes unwind dsDNA owing to their higher affinity towards ssDNA compared to dsDNA. The P-loop prototypes tended to adhere to the ELISA plates despite extensive washing, resulting in relatively high signal on the control, streptavidin-coated wells (*i.e.*, without DNA; **Supplementary figure 3C**). Yet, the binding signal from wells coated with ssDNA was consistently ≥2-fold higher than the background, while the signal from dsDNA-coated wells was equal or sometimes even lower than the background (**Supplementary figure 3C**).

Overall, we found that the core β-(P-loop)-α motif can be placed in a variety of structural contexts, with varying strand topologies, and yet retain, or even show improved biochemical function (**Figure 1D**, **Supplementary Figure S1**). This plasticity is likely the key to emergence of function in polypeptides. Given its minimal size and sequence complexity on the one hand, and its high expression, purity and foremost best strand separation activity, on the other, the N-αβα construct was employed as the representative P-loop prototype for the studies described below.

The N-αβα P-loop prototype shows avid and cooperative strand separation

Strand separation was dependent on the concentration of P-loop prototypes, in terms of both the rate and amplitude of fluorescence decay. At higher concentrations, the unwinding was faster and complete (*i.e.*, reached baseline) whereas at lower concentrations, unwinding was slower and partial (**Figure 2A, Supplementary Table S3B**). Binding isotherms obtained by plotting the end-

point fluorescence-decay values *versus* protein concentration indicated that strand separation is highly cooperative (sigmoidal curves and high Hill's coefficient) and occurs with apparent K_D values in the sub μM range (**Figure 2C**). The binding kinetics are complex since the dependence of the apparent rate constants on protein concentration was not linear (**Figure 2B**). Thus, strand separation appears to be a multiple step process. The rate determining step changes with protein concentration, and at > 0.5 μM becomes essentially concentration independent (**Figure 2B**). As shown later, both of these phenomena (cooperative isotherms and complex kinetics) are in agreement with changes in quaternary structure upon ligand binding.

Finally, mutations in the key P-loop residues of N-αβα reduced both the rate and the amplitude of fluorescence decay, and accordingly showed loss of binding to ssDNA by ELISA (**Supplementary Figure 3**).

ssDNA release upon NTP and polyphosphate binding

Strand-separation as shown so far is, in essence, a shift in equilibrium in favor of P-loop prototype bound ssDNA. However, helicases are enzymes that turnover, namely they also release the bound DNA, typically upon ATP hydrolysis. The P-loop prototypes bind ssDNA and ATP via the same P-loop motif as suggested by mutations in the P-loop residues that abrogated binding of both [16]. Based on this observation, we asked if ATP addition would release the ssDNA, thus also allowing the DNA to relax to its initial dsDNA state (**Figure 3A**). To this end, the N-αβα prototype was mixed with the beacon dsDNA and strand-separation was allowed to reach equilibrium. Upon subsequent addition of ATP and GTP, fluorescence reverted to its initial state indicating the release of the bound prototype and reversion to the starting dsDNA state (**Figure 3B**). Release by ATP occurred with an apparent K_D value in the range expected for a small ligand (K_D^{App} = 2.8 mM) and GTP showed 2-fold tighter binding (K_D^{App} = 1.4 mM; **Figure 3C**). It seems, however, that release of the ssDNA is primarily conferred by the triphosphate group of these NTPs, and not the nucleoside moiety, as indicated by even tighter binding of triphosphate (K_D^{App} = 790 μM). Given that inorganic phosphoanhydrides were proposed to have preceded NTPs as life's energy coin, we tested polyphosphate – Kornberg's energy fossil [32] – as well as hexametaphosphate. N-αβα showed a strong preference for both polyphosphates (K_D^{App} = 13.7 μM; calculated for an average of 18 phosphates per molecule, and 5.6 μM for hexametaphosphate; **Figure 3C**). Addition of phosphate at molar concentrations that are >100-fold higher than hexametaphosphate did not release the bound protein (5.6 mM phosphate barely had any effect on releasing the bound ssDNA, whereas 5.6 μM hexametaphosphate, equivalent to 33.6 μM phosphate, induced complete release; **Figure 3C**). Thus, regain of fluorescence seems to be driven by specific ligand binding rather than by nonspecific effects such as changes in ionic strength. The efficient release of prototype-bound ssDNA by hexametaphosphate was

further corroborated by ELISA experiments showing that prior incubation of N-αβα with hexametaphosphate, abrogated binding to 24 base ssDNA (**Figure 3D**).

The P-loop prototypes facilitate strand exchange

We further tested if N-αβα is able to unwind different types of DNA constructs and hence mediate strand exchanges of complementary DNA strands, *i.e.*, a recombinase-like function. To begin with, we assessed the ability of N-αβα to drive reversion from the quenched hairpin state to the fluorescent dsDNA state (**Figure 4A**). As expected, we observed an increase in fluorescence upon mixing the beacon oligo and its unlabeled anti-sense strand in equimolar concentration, since this is the thermodynamically favored outcome. However, this exchange was relatively slow, and did not reach a steady-state within the time frame of the experiment. Addition of N-αβα significantly accelerated it (**Figure 4B**).

In an alternative experiment, a dsDNA fragment comprising a fluoroscently labeled sense strand (FAM sense strand) hybridized to an unlabelled anti-sense stand was mixed with 10-fold molar excess of the anti-sense strand labelled with the quencher (BHQ-1 antisense strand; **Supplementary table S1**; **Figure 4C**). Although this reaction, similar to above, is thermodynamically favored, the strand-exchange that ultimately leads to the quenched dsDNA state is very slow and barely occurs on the experiement's timescale. This reaction was, however, signficantly accelarated by addition of N-αβα in a concentration dependent manner (**Figure 4D**). Finally, N-αβα does not quench the fluorescently labeled dsDNA in the absence of the quencher containing complementary strand (**Supplementary Figure 4**). This rules out the posibility that fluorescence quenching is driven by spurious interactions of the P-loop prototype with the fluorophore.

Quaternary structural plasticity

The intact P-loop prototypes tend to form dimers [16]. We assumed that their fragments are more likely to do so and possibly form even higher-order oligomers. Despite extensive attempts, we could not obtain crystals of N-αβα, or of any other functional construct described here. However, we performed chemical crosslinking experiments that revealed that N-αβα forms higher order oligomers, spanning from dimers to hexamers (**Supplementary Figure S2D**). Native mass spectrometry (MS) revealed that N-αβα self-assembles to form an ensemble of even higher-order forms, with the predominant and unambiguously assigned assemblies being 10-mer and 30-mer (**Figure 5A**). Furthermore, MS/MS experiments confirmed the identity of these species, as indicated, for example, by isolating the 30+ charge state of the 30-mer species, and inducing its dissociation into a highly charged monomer and a stripped 29-mer complex (**Figure 5B**).

Dynamic light scattering (DLS) measurements also indicated that N-αβα exists in a high oligomeric form (**Figure 5C)** with a Z-average diameter of 165 (±6) nm (**Supplementary Table S4**, the theoretical estimate for a monomer being < 10 nm). Addition of hexametaphosphate and polyphosphate increased the intensity of scattered light (**Figure 5C**) and suggested a further increase in particle diameter (**Figure 5C, 5D, Supplementary Table S4**). The sizes reported by DLS are only an approximation of the actual size. Nonetheless, the DLS results are in agreement with the apparent K_D values measured for various ligand (for ssDNA release, **Figure 3C**) - *i.e.*, GTP had a much weaker effect relative to ligands that promote polyvalent binding, such as hexametaphosphate and polyphosphate (**Figure 5B, 5C, Supplementary Table S4**).

Discussion

Previous studies have shown that NTP binding and modest catalysis can arise in polypeptides that comprise fragments of modern NTPases[16,33] and of similar folds [34]. This study extends our previous report [16] to demonstrate that polypeptides comprising the ancestral β-(P-loop)-α motif, with some minimal sequence additions to facilitate solubility, confers helicase-like functions. Our findings have several implications regarding the primordial P-loop NTPases, as discussed in the sections below.

From a generalist phospho-ligand binder to specialized enzymes

In contemporary helicases, translocases and RecA proteins, the P-loop mediates NTP binding and hydrolysis, while DNA binding is conferred by other surface loops or even by a separate domain [19–22]. In contrast, in our prototypes, the P-loop binds NTPs and inorganic polyphosphates, as well as nucleic acids. This multifunctionality is the key to the prototype's helicase-like action. Specifically, in the strand-exchange assays, the P-loop prototypes accelerate the rate of DNA rearrangements (**Figure 4**). Whereas, in unwinding experiments with beacon dsDNA, they merely shift the equilibrium toward ssDNA. However, their action can be reversed by addition of phospho-ligands such as ATP, and foremost by inorganic polyphosphates. These binding-release cycles are not enzymatic turnovers, yet may be a first step toward a *bona fide* helicase.

This multifunctionality is surprising, as although nucleic acids have phosphate groups, they fundamentally differ from NTPs. Can vestiges of a generalist P-loop, and specifically of ssRNA/DNA binding, be found in extant P-loop NTPases? We searched the PDB for domains that belong to P-loop NTPase lineage and have ssRNA/DNA bound in proximity to the P-loop (see Methods). This search identified at least two extant P-loop NTPase families: XPD helicase (**Figure 6A**), and polynucleotide kinase (**Figure 6B**), where the P-loop interacts with ssDNA, as it does in our P-loop prototypes. In the case of XPD helicase, the canonical Walker A motif diverged and phosphate binding is mediated by a short motif, SGR, at the tip of α1. Remarkably,

in case of polynucleotide kinase (**Figure 6B**), a canonical P-loop motif that connects to the tip of α1 binds GTP/GDP as well as ssDNA (oligonucleotide) by a network of interactions facilitated by the P-loop residues. This, to our knowledge, is the only instance of an extant multifunctional P-loop that not only catalyzes phosphoryl transfer, but also binds ssDNA.

At present, in the absence of structures at atomic resolution, the precise mode of binding by our P-loop prototypes remains unknown. It seems, however, that the Walker A motif is not critical per-se. Specifically, we observed that the first Gly of the Walker A motif of our P-loop prototypes plays no role, and that the last three residues (GK(S/T)) seem most critical; however, even at these three positions, mutations reduce but not completely abolish binding (see Ref. [16] and **Figure S3**). Indeed, the most rudimentary forms of phosphate binding make use of backbone amides, of glycine as well as other residues, and most critically, of bidentate interactions involving both backbone and side-chain H-bonds, foremost by Ser/Thr [14]. These elements are seen in XPD helicase (**Figure 6A**) and are likely to be the key to a generalist P-loop.

That the ancient P-loop was a 'generalist' that mediates multiple functions is in line with the hypothesis that the earliest enzymes were multifunctional [35]. A plausible explanation, in accord with the Dayhoff's hypothesis [3,4], is that such multi-functional primordial P-loop fragments were at a later stage duplicated and fused. This resulted in a tandem repeat of β-(P-loop)-α elements, where the P-loops comprise the active site. Further divergence allowed one P-loop to retain NTP binding and develop the ability to catalyze phosphoryl transfer, while the other P-loop(s) were repurposed to bind nucleic acids. This scenario is illustrated by XPD helicases wherein a P-loop ATPase domain, the DEAD domain (ECOD domain ID: e6fwrA2), is fused to the ssDNA binding helicase C_2 domain.

A minimal structural context for P-loop function

Bioinformatics analyses have pointed out the β-(P-loop)-α–β fragment as the recurrent structural/functional unit in dinucleotide binding proteins [5,36]. While we found that this fragment mediates strand separation, it was aggregation-prone, likely due to the highly hydrophobic β1 strand (**Supplementary table S2B**), and active only under non-stringent conditions. In contrast, the α–β-(P-loop)-α fragment was soluble and functional in the presence of salt. Having a helix preceding the β-(P-loop)-α fragment seems to present an advantage, primarily by enhancing solubility of this exceedingly hydrophobic $\beta\alpha$ fragment. We also note that although in most P-loop NTPase domains β1, from which the P-loop extends, comprises the N-terminus, an alpha helix that precedes β1 is also in some P-loop families, *e.g.* in the F-type ATP synthases (F-groups, ECOD: 2004.1.1.53; Pfam: PF00006), Transcription termination factor Rho (F-groups, ECOD: 2004.1.1.53; Pfam: PF00006), and RecA (F-groups, ECOD: 2004.1.1.237; Pfam: PF00154).

Moreover, the helicase-like function is retained despite truncation of most of this N-terminal helix, and even the β-(P-loop)-α fragment that could not be isolated was co-purified with bound nucleic acids. These results, along with the observation that ancestral β-(P-loop)-α motif can be embedded in various structural contexts while retaining function, suggest that β-(P-loop)-α is likely the minimal stand-alone seed from which P-loop NTPases could have emerged.

Dynamic self-assembly is key to function

We hypothesized that self-assembly is a critical bridging step that enables short polypeptides to be functional on their own prior to their duplication and fusion—a step that likely requires advanced genetic and protein translation machineries [4]. Shorter polypeptides are unlikely to confer biochemical functions such as small ligands binding [37]. However, self-assembly, even in rudimentary forms such as amyloid fibers [38,39] or coacervates [40], can provide the operative volume and network of interactions necessary for biochemical function [39,41]. Although further studies are required to elucidate the mechanistic and structural basis of these assemblies, the propensity of the P-loop prototypes to self-assemble is evident, as is the link between phospho-ligand binding and changes in assembly (**Figure 5**). Foremost, oligomerization confers avidity, *i.e.*, binding via multiple P-loops per functional unit. Otherwise, binding at μM affinity by a solvent exposed loop would have been impossible. Changes between oligomeric states are also indicated by the cooperativity of the strand separation reactions, as manifested in high Hill coefficients and complex kinetics (**Figure 2**). Similar DNA-induced cooperative functions are documented for SSB proteins [42], helicases [43,44] and RecA proteins [45–48], and the latter two are also P-loop NTPases. Further, RecA has been shown to also possess strand-separation activity on short dsDNAs [49], and its recombinase function involves changes in oligomeric states, from monomers-dimers up to long filaments [1,2].

The potential role of P-loop prototypes in the pre-LUCA world

Whether proteins or nucleic acids – metabolism or information storage – came first has been extensively debated. However, these scenarios are not necessarily mutually exclusive because both elements had to coexist in some rudimentary form before cellular forms emerged and gave rise to LUCA [50]. It is widely accepted that P-loop NTPases emerged early, possibly within an RNA-protein world [5,11–13,17,51,52]. Accordingly, RNA/DNA remodelers such as SFII helicases [52] and RecA constitute a major class of P-loop NTPases ascribed to the LUCA [7,8]. P-loop polypeptides may have therefore marked the early stages of cooperation between proteins and nucleic acids (other marked examples include polypeptides that interacted with ribosomal RNA [53–55]). Specifically, in the absence of protein-based polymerases, nucleic acids must have replicated either non-enzymatically [56,57] and/or in a self-catalytic manner [58]. However, in such scenarios, a

fundamental impediment for multiple rounds of replication is the stability of duplex RNA [59] (or DNA for that matter [60]). Heat can separate the strands, yet reannealing would be faster than any abiotic replication [61]. A plausible solution for unwinding RNA duplex products is short "invader" oligonucleotides [62]; however, how strand-displacement would initiate remains unresolved [62]. Thus, for multi-round replication, certainly of templates that are dozens of nucleotides long, an unwinding polypeptide is likely necessary. The duplex unwinding and strand displacement activities of our P-loop prototypes provide a plausible solution to these challenges. Thus, although much simpler in composition and smaller in size, these rudimentary P-loop forms hold tangible links in function, as well as in sequence, to their modern descendants.

Inorganic polyphosphates as energy fossils

Our P-loop prototypes bind phosphate moieties with no apparent interactions with the nucleoside (ATP, GTP and triphosphate bind similarly; **Figure 3**). Foremost, long chain polyphosphate binds with 1000-fold higher affinity than ATP. Indeed, inorganic phosphoanhydrides were proposed to have been the abiotic energy precursors of NTPs [63]. Of particular interest is hexametaphosphate – a cyclic ring of six phosphates that also binds with μM affinity (**Figure 3**). In the primitive biotic world, polyphosphates could have served not only as an energy source, but also as a scaffold that facilitated the assembly and orientation of phospholipids, nucleic acids and proteins [64]. Further, trimetaphosphate has been extensively explored as an abiotic condensation reagent that promotes synthesis of peptides and nucleic acids [65]. Trimetaphosphate binds weakly to our P-loop prototypes, but it coexists in equilibrium with hexametaphosphate [65] that binds at μM affinity (**Figure 3**). Thus, the mode of action of these P-loop prototypes is tantalizingly tailored to the requirements of a primordial world.

To conclude, Charles Darwin's immortal statement echoes: "from so simple a beginning endless forms most beautiful and most wonderful have been, and are being, evolved". The P-loop prototypes described here provide a glimpse of how these simple beginnings might have looked – short and simple polypeptides that are nonetheless linked to their modern descents in sequence, structure and function.

Materials and Methods

Protein expression and purification

Synthetic gene fragments encoding P-loop prototypes were purchased from *Twist Bioscience*. Cloning of synthetic genes and generation of mutant constructs, were performed as described previously [16]. All constructs had a C-terminal tag, comprising a Trp reside for concentration determination by measuring absorbance at 280 nm, (the P-loop prototypes have no aromatic

residues) followed by 6xHis for purification (amino acids and DNA sequences are provided in **Supplementary Table S1**). All proteins were expressed in *Escherichia coli* BL21 (DE3) cells. Cells were grown in LB media at 37 ºC with shaking (220 rpm) until OD600 ~0.6 and protein expression was induced by the addition of ITPG (1 mM final concentration) at 20 ºC. Following overnight induction at 20 ºC with shaking, cells were harvested by centrifugation (4000 g for 15 min at 4ºC) and resuspended in lysis buffer: 50 mM sodium phosphate, 20 mM imidazole, 500 mM NaCl, 6 M guanidine hydrochloride (pH 7.4), supplemented with the EDTA-free antiprotease cocktail supplied by Sigma. Cells were lysed by sonication, the debris was centrifuged down for 30 mins at 13000 rpm, and the supernatant was filtered through 0.22 µm membrane filter (Merck Millipore). Clarified lysates were loaded onto a HisTrapTM FF 5 mL column (GE Healthcare) using an AKTA FPLC. The guanidine hydrochloride that was added to dissociate bound nucleic acids was removed using a linear gradient of 12 column volumes of 50 mM sodium phosphate, 20 mM imidazole, 500 mM NaCl, pH 7.4. Bound proteins were eluted using one-step elution with 50 mM sodium phosphate, 500 mM imidazole, 500 mM NaCl, pH 7.4. Protein yield and purity was assessed by SDS-PAGE. Two rounds of dialysis were carried out to dialyze out the imidazole. The P-loop prototypes generally precipitated during the dialysis to remove imidazole. Precipitated protein samples were centrifuged, the pellet was collected and dissolved in buffer containing 50 mM Tris, 150 mM NaCl and 1 M L-arginine pH 8. Purified prototypes stored in this buffer at 4 °C, at 100 to 200 µM concentrations, remained mostly soluble and active for periods of seven to ten days.

Strand separation and exchange assays

Synthetic DNA oligonucleotides for unwinding and strand-exchange assays were obtained from Integrated DNA Technologies, Inc, and their sequences are listed in supplementary Table S1. The beacon dsDNA was prepared by hybridizing the beacon oligo (sense strand) and the unlabeled antisense oligo each at 10 µM in 50 mM Tris (pH 8). Hybridization was done by heating the oligo mixture at 95 °C for 5 mins followed by slow cooling overnight. Strand separation reactions were performed in a buffer containing 50 mM Tris (pH 8), and at the stringent binding conditions in 50 mM Tris (pH 8) with 100 mM NaCl. The reaction was initiated by adding P-loop prototypes (1 to 0.1 µM) to beacon dsDNA (5 nM) in 100 µl reaction volumes, at 24 °C, in Nunc-flat black 96-well plates. Fluorescence was monitored using Infinite M Plex microplate reader (TECAN) with an excitation/emission wavelength of 495/540 nm. Fluorescence decay values were normalized to the initial fluorescence before protein addition (F_0) to obtain F/F_0 values. The non-specific quenching values observed with 5 nM of beacon DNA digested overnight with Benzonase (Merck Millipore) was subtracted from the proteinderived signals. Rate constants were determined by fitting the time dependent F/F_0 values to one-phase (Eq. 1).

(1) $F/F_{0\ (t)} = (F/F_0)^{\infty} + (1 - (F/F_0)^{\infty}) \times e^{-kapp*t}$

where t is time, $(F/F_0)^{\infty}$ is the end-point value of F/F_0, $kapp$ is the apparent first-order rate constant.

For determining apparent binding affinities, the end-point F/F_0 values from the strand-separation experiments were derived for each protein concentration (P), and normalized (0 = the starting, fluorescent beacon substrate; 1 = the assay baseline, i.e., the fully quenched hairpin state). Normalized F/F_0 values were then plotted against protein concentration. The resulting data were fitted to a binding isotherm equation (Eq. 2; GraphPad Prism) with cooperativity, to derive the apparent dissociation constant (K_D^{App}) and the Hill coefficient (h).

(2) $F/F_{0\ (P)} = [P]^h/(K_D^{App} + [P]^h)$

Strand exchange assays were carried out in 50 mM Tris (pH 8) with 100 mM NaCl. For strand-exchange reactions with the quenched hairpin, the molecular beacon oligo (sense strand) was heated at 95 °C for 5 mins and renatured by slow cooling (3-4 hrs.) to room temperature yielding a hairpin structure due to the 4 base-complementary regions (**Supplementary Table S1**). To a premix of this quenched hairpin (5 nM) and P-loop prototypes (0.5 to 20 μM), an equimolar mixture of the unlabeled antisense strand (**Supplementary Table S1**) was added, in 100 μl volumes, to initiate the reaction and change in fluorescence was monitored. For reactions with dsDNA, a dsDNA stock was prepared by hybridizing the FAM sense strand (Supplementary Table S1) and the unlabeled antisense strand in 50 mM Tris pH 8, at 10 μM each, by heating and slow cooling as above. A mixture of this hybridized dsDNA (5 nM) and the BHQ-1 antisense strand (50 nM) was then used as the DNA substrate and reactions were initiated by adding P-loop prototypes (1 and 0.5 μM). Changes in fluorescence were normalized to the initial state (prior to protein addition) and data were fit to Eq. 1 as described above.

For determining apparent binding affinities of phospho-ligands, the fraction of released ssDNA (**Figure 3B**), for each ligand concentration (P), was normalized (1 = complete release and reversion of ssDNA to the starting, fluorescent beacon dsDNA substrate; 0 = no release, i.e., without added ligand). Normalized F/F_0 values were then plotted against the ligand concentration and the resulting data were fitted to a binding isotherm equation with cooperativity as described above (Eq. 2), to derive the apparent dissociation constant (K_D^{App}) and the Hill coefficient (h).

Enzyme-linked immunosorbent assay (ELISA)

ELISA experiments were performed as previously described [16] with some modifications. Stock solutions of 24 bp biotinylated dsDNA were prepared by hybridizing (see above) equimolar concentrations (100 μM) of biotinylated-24nt-ssDNA with the unlabeled (antisense) strand in

buffer containing 50 mM sodium phosphate and 100 mM NaCl; pH 7 (oligo sequences are listed in **Supplementary Table S1**). Streptavidin coated plates (*StreptaWell, Roche*) were coated with 100 µl of 0.05 µM of biotinylated 24 bp dsDNA, or biotinylated-24nt-ssDNA, diluted in ELISA buffer (50 mM sodium phosphate and 100 mM NaCl; pH 7. and 1 % non-ionic detergent Nonidet P40 and 0.1% BSA, pH 7) for 1 hr at ambient temperature. In parallel, wells for background subtraction were left uncoated (incubated with 100 µl ELISA buffer). Following coating, wells were washed with ELISA buffer and 100 µl of P-loop prototypes solutions were added (at 0.25 to 0.06 µM) to both DNA-coated and background wells, and incubated for 1 hr. The unbound proteins were washed extensively with ELISA buffer (10 times) and 100 µl of 0.1 µg/ml HRP labeled mouse anti-His antibody (200 µg/ml, Santa Cruz Biotechnology) were added and incubated for 40 mins. The wells were washed extensively, 100 µl of substrate solution containing 1.25 mMol/L TMB and 2.21 mMol/L hydrogen peroxide, <1% dimethyl sulfoxide in 0.08 Mol/L acetate buffer at pH 4.9 (3, 3', 5, 5'-tetramethybenzidine; TMB; ES001, Millipore) was added and absorbance at 650 nm was monitored for 30 mins. The results are presented as endpoint values of OD^{650nm} after subtraction of the background signal.

Chemical crosslinking

Chemical crosslinking of P-loop prototypes was performed with EDC (1-ethyl-3-(3-dimethylaminopropyl) carbodiimide, hydrochloride salt) [66]. Reactions were carried out as follows: purified P-loop prototypes were dialyzed against 10 mM MES buffer pH 4.5, and diluted to 30 µM concentration in the same buffer. In 20 µl reaction volumes, 30 µM of protein were mixed with EDC (10 to 60 mM final concentration) dissolved in the above buffer. Reactions were incubated for 30 mins at room temperature and quenched with adding 50-fold molar excess (over cross-linker concentration) of Tris buffer pH 8. Samples were mixed with SDS loading dye and analyzed on 16% SDS-PAGE gels run with Tris-glycine buffer.

Dynamic light scattering (DLS)

DLS analysis of N-$\alpha\beta\alpha$ construct was performed using Malvern Zetasizer Nano-ZS particle analyzer (*Malvern Panalytical*). The P-loop prototypes were diluted to 1 µM in 50 mM Tris, 100 mM NaCl pH 8. Following an equilibration time of 2 min, light scattering was monitored in a disposable cuvette in 1 ml volumes at 25 °C. The measurement duration was set to 'automatic', resulting in 11 to 17 runs for each measurement and three measurements were performed for each sample. The data were fit to a correlation function and analyzed by the method of cumulants [67] to obtain the z-average diameter (nm) (i.e. mean particle size). To test the effect of phospho-ligands, the prototype was mixed with different phosphate ligands, and light scattering was monitored as described above to obtain the Z-average diameter.

Native mass spectrometry analysis

Nanoflow electrospray ionization MS and tandem MS experiments were conducted under nondenaturing conditions on a Q Exactive UHMR Hybrid Quadrupole-Orbitrap mass spectrometer (Thermo Fisher Scientific). Prior to MS analysis, the purified N-αβα was dialyzed against 150 mM ammonium acetate (pH 7.5) and diluted to a final concertation of 10 µM. Spectra were collected under positive ion mode, and conditions were optimized to enable the ionization and removal of adducts while retaining the noncovalent interactions of the proteins tested. In MS/MS experiments, the relevant m/z values were isolated and argon gas was admitted to the collision cell. Typically, aliquots of 2 µL of sample were electrosprayed from gold-coated borosilicate capillaries prepared in-house [68]. Spectra are shown using UniDec [69] for mass detection, and without smoothing or background subtraction.

The following experimental parameters were used on the UHMR Hybrid Quadrupole-Orbitrap platform: spray voltage 1.35 kV, inlet capillary temperature 250 °C. The trapping gas pressure was set to 5 corresponding to HV pressures of 1.5x10-4 mbar. To facilitate efficient desolvation of proteins, in source trapping was set to -100 V and high-energy collision dissociation was set to -10 eV. Mass spectra were recorded at a resolution of 3,125. Injection flatapole DC bias was set to 5 V. For tandem MS the precursor (6,540 m/z) was isolated and activated using the HCD cell at 100 eV. Instruments were externally mass-calibrated using a cesium iodide solution at a concentration of 2 mg/mL.

Identification of ssDNA binding by P-loop NTPases

All structures annotated by the ECOD database (version develop275) as containing a P-Loop domain (X-group 2004) were downloaded from the Protein Data Bank – 5,818 structures in total. Structures in which a P-Loop domain and ssDNA come within 3.5 Å of each other were identified using a short script implemented in Python. Hits were validated by visual inspection.

Acknowledgments

This research is funded by a Minerva Foundation grant for scientific cooperation between Germany and Israel. We thank Dr. Guy Shmul for help with DLS analysis and for providing size standards and Dr. Gili Ben-Nissan for help with native mass-spectrometry experiments. Schematics for strand-separation, strand exchange and release assays were created with BioRender.com.

References

1. Bell JC, Kowalczykowski SC. RecA: Regulation and Mechanism of a Molecular Search Engine. *Trends Biochem Sci*. 2016;41(6):491-507. doi:10.1016/j.tibs.2016.04.002

2. Bleichert F, Botchan MR, Berger JM. Mechanisms for initiating cellular DNA replication. *Science (80-)*. 2017;355(6327):eaah6317. doi:10.1126/science.aah6317

3. Eck R V, Dayhoff MO. Evolution of the structure of ferredoxin based on living relics of primitive amino Acid sequences. *Science*. 1966;152(3720):363-366. doi:10.1126/science.152.3720.363

4. Romero MLR, Rabin A, Tawfik DS. Functional Proteins from Short Peptides : Dayhoff s Hypothesis Turns 50. *Angew Chem Int Ed Engl*. 2016;1980:15966-15971. doi:10.1002/anie.201609977

5. Alva V, Söding J, Lupas AN. A vocabulary of ancient peptides at the origin of folded proteins. *Elife*. 2015;4(DECEMBER2015):1-19. doi:10.7554/eLife.09410.001

6. Walker JE, Saraste M, Runswick MJ, Gay NJ. Distantly related sequences in the alpha- and beta-subunits of ATP synthase, myosin, kinases and other ATP-requiring enzymes and a common nucleotide binding fold. *EMBO J*. 1982;1(8):945-951.

7. Leipe DD, Wolf YI, Koonin E V., Aravind L. Classification and evolution of P-loop GTPases and related ATPases. *J Mol Biol*. 2002;317(1):41-72. doi:10.1006/jmbi.2001.5378

8. Leipe DD, Koonin E V., Aravind L. Evolution and classification of P-loop kinases and related proteins. *J Mol Biol*. 2003;333(4):781-815. doi:10.1016/j.jmb.2003.08.040

9. Saraste M, Sibbald PR, Wittinghofer A. The P-loop — a common motif in ATP- and GTP-binding proteins. *Trends Biochem Sci*. 1990;15(11):430-434. doi:https://doi.org/10.1016/0968-0004(90)90281-F

10. Ogura T, Wilkinson AJ. AAA+ superfamily ATPases: common structure–diverse function. *Genes to Cells*. 2001;6(7):575-597. doi:10.1046/j.1365-2443.2001.00447.x

11. Koonin E V, Wolf YI, Aravind L. Protein fold recognition using sequence profiles and its application in structural genomics. *Adv Protein Chem*. 2000;54:245-275.

12. Söding J, Lupas AN. More than the sum of their parts: On the evolution of proteins from peptides. *BioEssays*. 2003;25(9):837-846. doi:10.1002/bies.10321

13. Ma B, Chen L, Ji H, et al. Characters of very ancient proteins. *Biochem Biophys Res Commun*. 2008;366(3):607-611. doi:10.1016/j.bbrc.2007.12.014

14. Longo LM, Petrović D, Kamerlin SCL, Tawfik DS. Short and simple sequences favored the emergence of N-helix phospho-ligand binding sites in the first enzymes. *Proc Natl Acad Sci*. 2020;117(10):5310 LP - 5318. doi:10.1073/pnas.1911742117

15. Watson JD, Milner-White EJ. A novel main-chain anion-binding site in proteins: the nest. A particular combination of phi,psi values in successive residues gives rise to anion-binding sites that occur commonly and are found often at functionally important regions. *J Mol Biol*. 2002;315(2):171—182. doi:10.1006/jmbi.2001.5227

16. Romero Romero ML, Yang F, Lin Y-R, et al. Simple yet functional phosphate-loop proteins. *Proc Natl Acad Sci*. 2018;115(51):E11943 LP-E11950. doi:10.1073/pnas.1812400115

17. Berezovsky IN. Towards descriptor of elementary functions for protein design. *Curr Opin Struct Biol*. 2019;58:159-165. doi:https://doi.org/10.1016/j.sbi.2019.06.010

18. Laurino P, Tóth-Petróczy Á, Meana-Pañeda R, Lin W, Truhlar DG, Tawfik DS. An Ancient Fingerprint Indicates the Common Ancestry of Rossmann-Fold Enzymes Utilizing Different Ribose-Based Cofactors. *PLOS Biol*. 2016;14(3):e1002396. https://doi.org/10.1371/journal.pbio.1002396.

19. Weinstock GM, McEntee K, Lehman IR. ATP-dependent renaturation of DNA catalyzed by the recA protein of Escherichia coli. *Proc Natl Acad Sci*. 1979;76(1):126 LP - 130. doi:10.1073/pnas.76.1.126

20. Menetski JP, Bear DG, Kowalczykowski SC. Stable DNA heteroduplex formation catalyzed by the Escherichia coli RecA protein in the absence of ATP hydrolysis. *Proc Natl Acad Sci*. 1990;87(1):21-25. doi:10.1073/PNAS.87.1.21

21. Gorbalenya AE, Koonin E V. Helicases: amino acid sequence comparisons and structure-function relationships. *Curr Opin Struct Biol*. 1993;3(3):419-429. doi:10.1016/S0959-440X(05)80116-2

22. Prentiss M, Prévost C, Danilowicz C. Structure/function relationships in RecA protein-mediated homology recognition and strand exchange. *Crit Rev Biochem Mol Biol*. 2015;50(6):453-476. doi:10.3109/10409238.2015.1092943

23. Saraste M, Sibbald PR, Wittinghofer A. The P-loop - a common motif in ATP- and GTP-binding proteins. *Trends Biochem Sci*. 2017;15(11):430-434. doi:10.1016/0968-0004(90)90281-F

24. Iyer LM, Leipe DD, Koonin E V, Aravind L. Evolutionary history and higher order classification of AAA+ ATPases. *J Struct Biol*. 2004;146(1-2):11-31. doi:10.1016/j.jsb.2003.10.010

25. Mulkidjanian AY, Makarova KS, Galperin MY, Koonin E V. Inventing the dynamo machine: the evolution of the F-type and V-type ATPases. *Nat Rev Microbiol*. 2007;5(11):892-899. doi:10.1038/nrmicro1767

26. von Hippel PH, Johnson NP, Marcus AH. Fifty years of DNA “breathing”: Reflections on old and new approaches. *Biopolymers*. 2013;99(12):923-954. doi:10.1002/bip.22347

27. Phelps C, Lee W, Jose D, von Hippel PH, Marcus AH. Single-molecule FRET and linear dichroism studies of DNA breathing and helicase binding at replication fork junctions. *Proc Natl Acad Sci*. 2013;110(43):17320 LP - 17325. doi:10.1073/pnas.1314862110

28. Fei J, Ha T. Watching DNA breath one molecule at a time. *Proc Natl Acad Sci*. 2013;110(43):17173 LP - 17174. doi:10.1073/pnas.1316493110

29. Lionnet T, Spiering MM, Benkovic SJ, Bensimon D, Croquette V. Real-time observation of bacteriophage T4 gp41 helicase reveals an unwinding mechanism. *Proc Natl Acad Sci*. 2007;104(50):19790 LP - 19795. doi:10.1073/pnas.0709793104

30. Belon CA, Frick DN. Monitoring Helicase Activity With Molecular Beacons. *Biotechniques*. 2009;45(4):433-442. doi:10.2144/000112834.Monitoring

31. Koga N, Tatsumi-Koga R, Liu G, et al. Principles for designing ideal protein structures. *Nature*. 2012;491(7423):222-227. doi:10.1038/nature11600

32. Kornberg A. Inorganic polyphosphate: Toward making a forgotten polymer unforgettable. *J Bacteriol*. 1995;177(3):491-496. doi:10.1128/jb.177.3.491-496.1995

33. Chuang WJ, Abeygunawardana C, Gittis AG, Pedersen PL, Mildvan AS. Solution Structure and Function in Trifluoroethanol of PP-50, an ATP-Binding Peptide from F1ATPase. *Arch Biochem Biophys*. 1995;319(1):110-122. doi:https://doi.org/10.1006/abbi.1995.1272

34. Pham Y, Kuhlman B, Butterfoss GL, Hu H, Weinreb V, Carter CWJ. Tryptophanyl-tRNA synthetase Urzyme: a model to recapitulate molecular evolution and investigate intramolecular complementation. *J Biol Chem*. 2010;285(49):38590-38601. doi:10.1074/jbc.M110.136911

35. Roy A. Jensen. Enzyme Recruitment in Evolution of New Function. *Annu Rev Microbiol*. 1976;(30):409-425.

36. Wierenga RK, De Maeyer MCH, Hoi WGJ. Interaction of Pyrophosphate Moieties with α-Helixes in Dinucleotide Binding Proteins. *Biochemistry*. 1985;24(6):1346-1357. doi:10.1021/bi00327a012

37. Corey DR, Phillips MA. Cyclic peptides as proteases: a reevaluation. *Proc Natl Acad Sci*. 1994;91(10):4106 LP - 4109. doi:10.1073/pnas.91.10.4106

38. Greenwald J, Riek R. On the Possible Amyloid Origin of Protein Folds. *J Mol Biol*. 2012;421(4):417-426. doi:https://doi.org/10.1016/j.jmb.2012.04.015

39. Rufo CM, Moroz YS, Moroz O V, et al. Short peptides self-assemble to produce catalytic amyloids. *Nat Chem*. 2014;6(4):303-309. doi:10.1038/nchem.1894

40. Longo LM, Despotović D, Weil-Ktorza O, et al. Primordial emergence of a nucleic acid binding protein via phase separation and statistical ornithine to arginine conversion. *Proc Natl Acad Sci*. January 2020:2020.01.18.911073. doi:10.1101/2020.01.18.911073

41. Makhlynets O V, Gosavi PM, Korendovych I V. Short Self-Assembling Peptides Are Able to Bind to Copper and Activate Oxygen. *Angew Chem Int Ed Engl*. 2016;55(31):9017-9020. doi:10.1002/anie.201602480

42. Dubiel K, Myers AR, Kozlov AG, et al. Structural Mechanisms of Cooperative DNA Binding by Bacterial Single-Stranded DNA-Binding Proteins. *J Mol Biol*. 2019;431(2):178-195. doi:10.1016/j.jmb.2018.11.019

43. Lee N-R, Kwon H-M, Park K, Oh S, Jeong Y-J, Kim D-E. Cooperative translocation enhances the unwinding of duplex DNA by SARS coronavirus helicase nsP13. *Nucleic*

Acids Res. 2010;38(21):7626-7636. doi:10.1093/nar/gkq647

44. Byrd AK, Raney KD. Increasing the Length of the Single-Stranded Overhang Enhances Unwinding of Duplex DNA by Bacteriophage T4 Dda Helicase. *Biochemistry*. 2005;44(39):12990-12997. doi:10.1021/bi050703z

45. Lehman MC and IR. recA Protein-promoted DNA Strand Exchange. *J Biol Chem*. 1982;257(14):8523-8532.

46. Cox MM. Motoring along with the bacterial RecA protein. *Nat Rev Mol Cell Biol*. 2007;8(2):127-138. doi:10.1038/nrm2099

47. Kowalczykowski SC. Structural biology: Snapshots of DNA repair. *Nature*. 2008;453(7194):463-466. doi:10.1038/453463a

48. Ragunathan K, Joo C, Ha T. Real-time observation of strand exchange reaction with high spatiotemporal resolution. *Structure*. 2011;19(8):1064-1073. doi:10.1016/j.str.2011.06.009

49. Bianchi M, Riboli B, Magni G. E. coli recA protein possesses a strand separating activity on short duplex DNAs. *EMBO J*. 1985;4(11):3025-3030. https://pubmed.ncbi.nlm.nih.gov/3905387.

50. Preiner M, Asche S, Becker S, et al. The future of origin of life research: Bridging decades-old divisions. *Life*. 2020;10(3). doi:10.3390/life10030020

51. Goncearenco A, Berezovsky IN. Protein function from its emergence to diversity in contemporary proteins. *Phys Biol*. 2015;12(4):45002. doi:10.1088/1478-3975/12/4/045002

52. Anantharaman V, Koonin E. V AL. Comparative genomics and evolution of proteins involved in RNA metabolism. *Nucleic Acids Res*. 2002;30(7):1427-1464. doi:10.1093/nar/30.7.1427

53. Lupas AN, Alva V. Ribosomal proteins as documents of the transition from unstructured (poly)peptides to folded proteins. *J Struct Biol*. 2017;198(2):74-81. doi:https://doi.org/10.1016/j.jsb.2017.04.007

54. Lanier KA, Roy P, Schneider DM, Williams LD. Ancestral Interactions of Ribosomal RNA and Ribosomal Proteins. *Biophys J*. 2017;113(2):268-276. doi:https://doi.org/10.1016/j.bpj.2017.04.007

55. Frenkel-Pinter M, Haynes JW, Mohyeldin AM, et al. Mutually stabilizing interactions between proto-peptides and RNA. *Nat Commun*. 2020;11(1):3137. doi:10.1038/s41467-020-16891-5

56. Deck C, Jauker M, Richert C. Efficient enzyme-free copying of all four nucleobases templated by immobilized RNA. *Nat Chem*. 2011;3(8):603-608. doi:10.1038/nchem.1086

57. Adamala K, Szostak JW. Nonenzymatic template-directed RNA synthesis inside model protocells. *Science*. 2013;342(6162):1098-1100. doi:10.1126/science.1241888

58. Bartel DP, Doudna JA, Usman N, Szostak JW. Template-directed primer extension catalyzed by the Tetrahymena ribozyme. *Mol Cell Biol*. 1991;11(6):3390-3394. doi:10.1128/mcb.11.6.3390

59. Ross PD, Sturtevant JM. THE KINETICS OF DOUBLE HELIX FORMATION FROM POLYRIBOADENYLIC ACID AND POLYRIBOURIDYLIC ACID. *Proc Natl Acad Sci U S A*.

1960;46(10):1360-1365. doi:10.1073/pnas.46.10.1360

60. Teichert JS, Kruse FM, Trapp O. Direct Prebiotic Pathway to DNA Nucleosides. *Angew Chemie Int Ed*. 2019;58(29):9944-9947. doi:10.1002/anie.201903400

61. Szostak JW. The eightfold path to non-enzymatic RNA replication. *J Syst Chem*. 2012;3(1):2. doi:10.1186/1759-2208-3-2

62. Zhou L, Kim SC, Ho KH, et al. Non-enzymatic primer extension with strand displacement. Nilsen TW, Marletta MA, Nilsen TW, Chaput JC, eds. *Elife*. 2019;8:e51888. doi:10.7554/eLife.51888

63. Kornberg A, Rao NN, Ault-riché D. Inorganic Polyphosphate : A MOLECULE OF MANY FUNCTIONS. 1999:89-125.

64. Brown MRW, Kornberg A. Inorganic polyphosphate in the origin and survival of species. *Proc Natl Acad Sci*. 2004;101(46):16085-16087.

65. Baccolini G. The Possible Role of Cyclic Pentacoordinate Phosphorus Intermediates in the Origin and Evolution of Life. are Phosphoric Anhydride and Trimetaphosphates Prebiotic Reagents? *Phosphorus Sulfur Silicon Relat Elem*. 2015;190(12):2173-2186. doi:10.1080/10426507.2015.1083569

66. Lepvrier E, Doigneaux C, Moullintraffort L, Nazabal A, Garnier C. Optimized protocol for protein macrocomplexes stabilization using the EDC, 1-ethyl-3-(3-(dimethylamino)propyl)carbodiimide, zero-length cross-linker. *Anal Chem*. 2014;86(21):10524-10530. doi:10.1021/ac502561e

67. Koppel DE. Analysis of Macromolecular Polydispersity in Intensity Correlation Spectroscopy: The Method of Cumulants. *J Chem Phys*. 1972;57(11):4814-4820. doi:10.1063/1.1678153

68. Kirshenbaum N, Michaelevski I, Sharon M. Analyzing large protein complexes by structural mass spectrometry. *J Vis Exp*. 2010;(40). doi:10.3791/1954

69. Marty MT, Baldwin AJ, Marklund EG, Hochberg GKA, Benesch JLP, Robinson C V. Bayesian Deconvolution of Mass and Ion Mobility Spectra: From Binary Interactions to Polydisperse Ensembles. *Anal Chem*. 2015;87(8):4370-4376. doi:10.1021/acs.analchem.5b00140

Figures

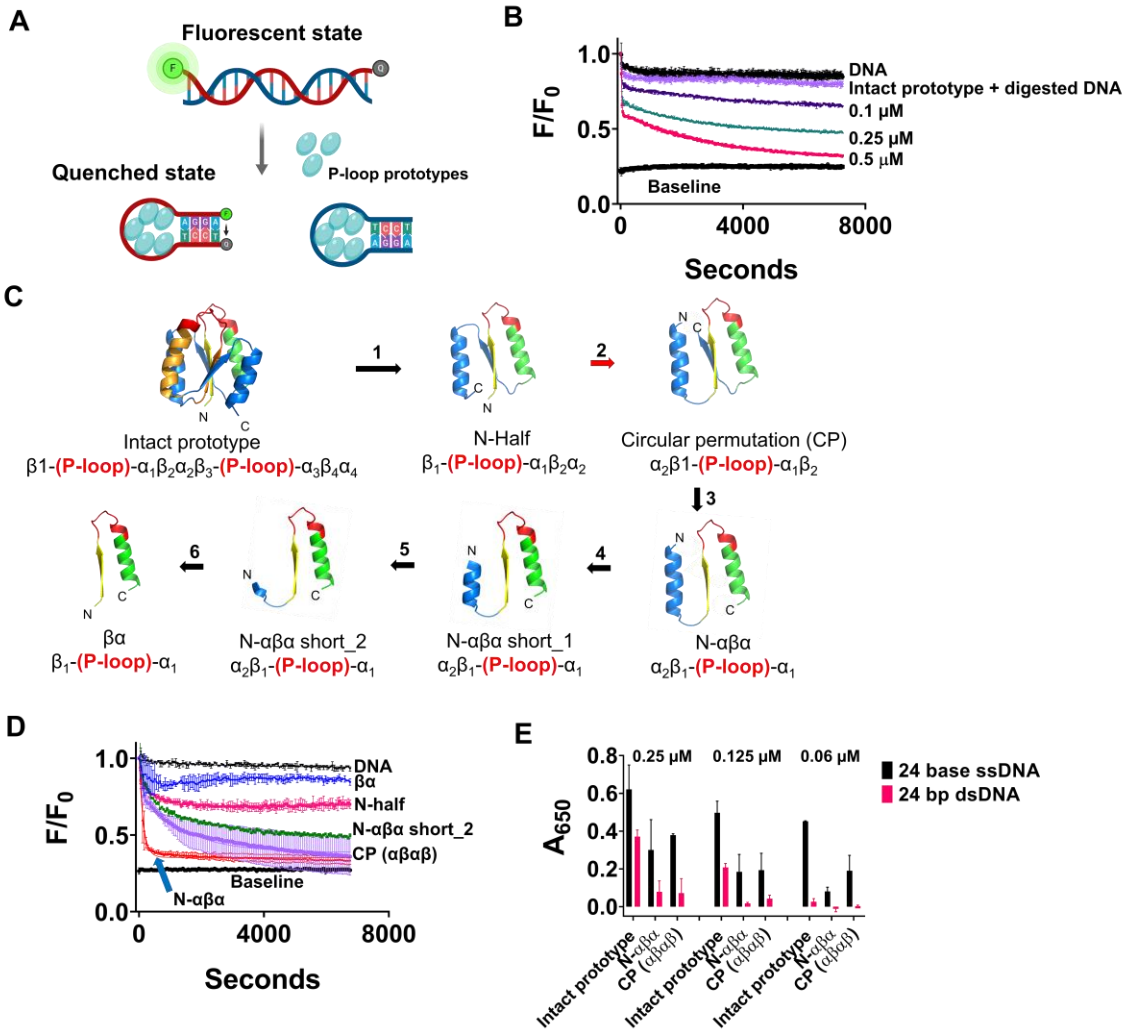

Figure 1. The molecular beacon assay reports the strand separation of P-loop prototypes.

A. Simplified schematic of the strand-separation molecular beacon assay [30]**.** In the initial dsDNA state, the quencher of the beacon strand is held apart from the fluorophore resulting in energy transfer (high fluorescence). The preferential binding of P-loop prototypes to ssDNA induces strand separation, allowing the beacon strand to assume a hairpin state wherein the fluorophore is quenched.

B. A representative strand separation experiment using the intact 110 residue P-loop prototype (D-Ploop; Ref [16]). Strand separation is reported by the change in FRET signal upon addition of the P-loop prototype at increasing protein concentrations. All assays were performed with 5 nM beacon dsDNA, in 50 mM Tris pH 8, at 24 °C. Shown are normalized F/F_0 values,

whereby the initial fluorescence of beacon dsDNA prior to protein addition takes the value of 1. Baseline represents the signal of the fully quenched hairpin beacon. Digested DNA represents the signal upon addition of 0.5 μM P-loop prototype to the beacon dsDNA pretreated with Benzonase nuclease. Traces were fitted to a biphasic exponential decay model (described in 'Supplementary Information' section) and the apparent rate constants are given in **Supplementary Table S3A**.

C. New P-loop prototypes were constructed by systematic truncation and circular permutation of the intact prototype.The numbered arrows indicate sequential steps in the engineering of new constructs as follows: *1.* Truncation of the intact 110 residue prototype into half [16] (N-half indicates N-terminal half). *2.* Circular permutation (red arrow) of N-half to a construct with 'αβαβ' architecture. *3.* Truncation of the C-terminal β-strand to give N-αβα. *4-6.* Incremental truncations of N-terminal helix of N-αβα down to a βα fragment. The structural models indicate the ancestral P-loop element in yellow (β1), red (the Walker P-loop) and green (α1), while the remaining parts are in blue.

D. Strand separation by truncated P-loop prototypes, at 1 μM protein concentration, and under the stringent condition (plus 100 mM NaCl; other assay conditions as in panel A).

E. Binding of P-loop prototypes to ssDNA or dsDNA as tested by ELISA. Biotinylated 24-base DNAs were immobilized to streptavidin-coated plates and prototype binding (at 0.25, 0.125 and 0.06 μM concentration) was detected with anti-His-HRP conjugated antibodies and by monitoring blue color formation at 650 nm due to oxidation of TMB substrate (See 'Methods' and **Supplementary Figure S3C**).

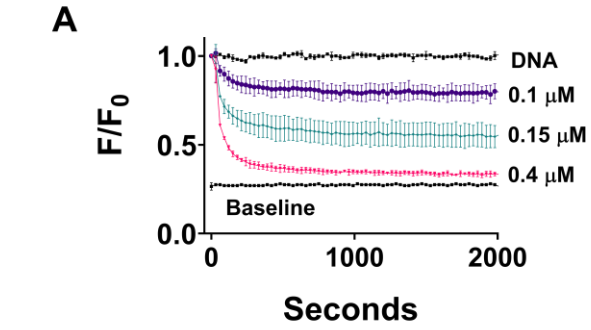

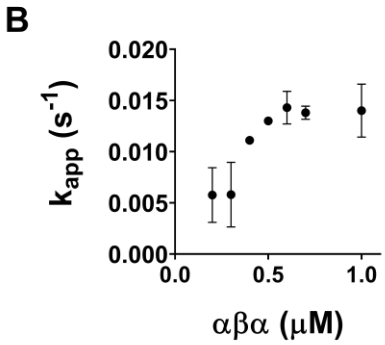

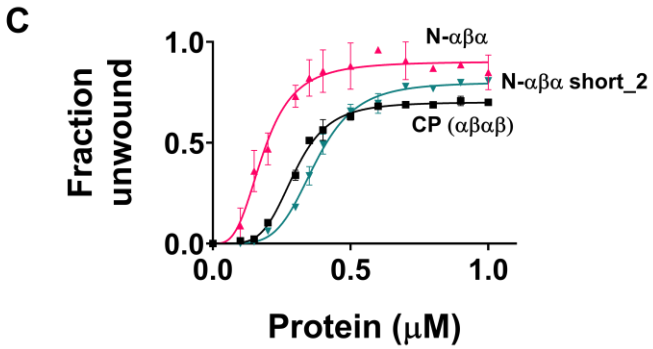

Protein	K_D^{app} (μM)	h
CP (αβαβ)	0.372 (±0.007)	4.7 (±0.2)
N-αβα	0.181 (±0.025)	4 (±1)
N-αβα short_2	0.296 (±0.010)	5 (±1)

Figure 2. Binding affinities and kinetics of strand-separation by P-loop prototypes.

A. A representative strand-separation experiment with varying concentrations of N-αβα (assay conditions as in **Figure 1D**). Shown are the average values from 2-6 independent runs, with the vertical bars representing the SD values. Traces were fitted to a one phase exponential decay model (Eq. 1, Methods) and the apparent rate constants are given in **Supplementary Table S3**.

B. The apparent rate constants plotted against protein concentration.

C. Binding isotherms of P-loop prototypes (for their topology, see **Figure 1C**). End-point F/F_0 values from strand separation experiments (*e.g.* panel A) were normalized (fluorescence of

the starting beacon dsDNA equals 0, and of the fully quenched ssDNA hairpin equals 1) to derive the relative fraction of unwound dsDNA, and were then plotted vs. protein concentration. Apparent binding affinities (K_D^{app}) and hill's coefficient (h) were calculated using Eq. 2 (Methods). The vertical error bars, and the numbers in parenthesis in the table, represent the standard deviation from 2-6 independent experiments.

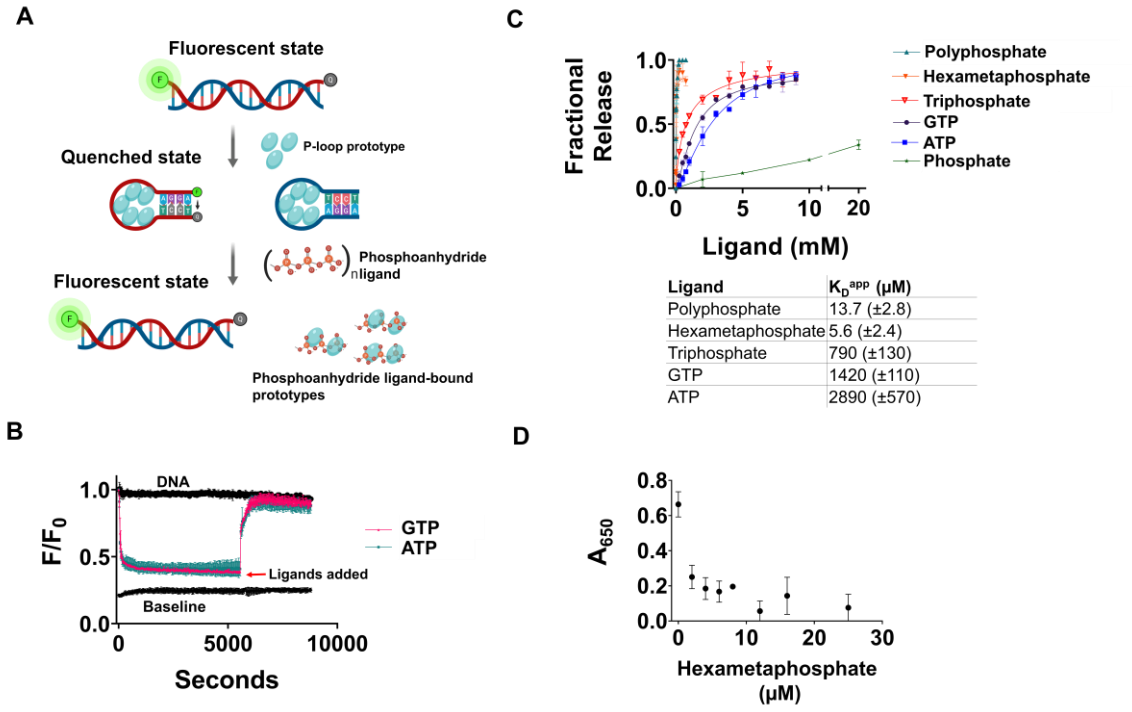

Ligand	K_D^{app} (μM)
Polyphosphate	13.7 (±2.8)
Hexametaphosphate	5.6 (±2.4)
Triphosphate	790 (±130)
GTP	1420 (±110)
ATP	2890 (±570)

Figure 3: Release of bound ssDNA by phosphoranhydride ligands.

A. A schematic description of the induction of strand separation by a P-loop prototype (step 1) followed by the displacement of the bound ssDNA by various phosphoanhydrides (P_n) and relaxation to the initial dsDNA state (step 2).

B. Representative strand separation experiments with 0.4 μM N-αβα added at time zero. Subsequent addition of ATP (turquoise) and GTP (pink, both at 9 mM concentration) leads to the release of the bound ssDNA and its relaxation to the initial dsDNA state.

C. The apparent affinities (K_D^{App}) of binding of various phosphoanhydride ligands to P-loop prototype N-αβα. The fraction of released ssDNA upon addition of phospho-ligands was calculated by normalizing the F/F_0 values from the plot in panel B, such that complete release (=1) corresponds to the initial unbound dsDNA state and, no release (=0) corresponds to the steady-state value of F/F_0 prior to ligand addition. The apparent binding affinities (K_D^{app}) were calculated by Eq. 2 (see Methods). Vertical error bars, and values in parenthesis, represent standard deviation from two independent experiments.

D. Inhibition of ssDNA binding. Preincubation of 0.125 μM N-αβα with increasing concentrations of hexametaphosphate shows abrogation of binding to 24 base biotinylated ssDNA in an ELISA-format.

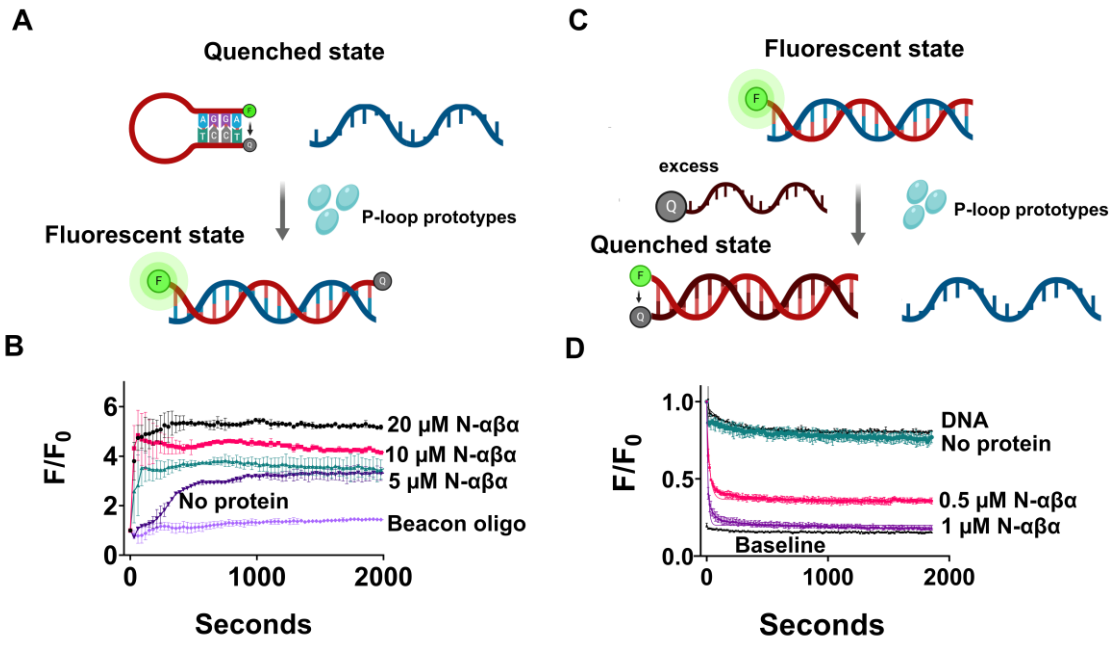

Figure 4. The N-αβα P-loop prototype mediates strand exchanges.

A. A schematic of the strand exchange reaction. Addition of the complementray strand to the beacon hairpin results in an exchange from an intra-molecular to inter-molecular dsDNA interaction. The latter involves a longer dsDNA stretch and is thus thermodynamically favored.

B. The exchange reaction was monitored by loss of FRET (increase in fluorescence) upon addition of the complementary antisense strand to a premix of the quenched hairpin beacon and N-αβα. Normalized fluorescence (F/F_0) was plotted vs. time (the purple line, beacon oligo, represents the quenched hairpin on its own). All strand-exchange assays were carried out in the presence of 100 mM NaCl, at 24 °C.

C. A schematic of the strand exchange reaction between a quencher containing anti-sense strand and its unlabelled analogue.

D. Induction of FRET was monitored upon addition of N-αβα to a premix of fluorescently labeled dsDNA and 10-fold excess of BHQ-1 anti-sense strand. Shown are the average values from 2-3 independent runs, with the vertical error bars representing the standard deviation values. Data were fit to a one-phase exponential decay (Eq. 1).

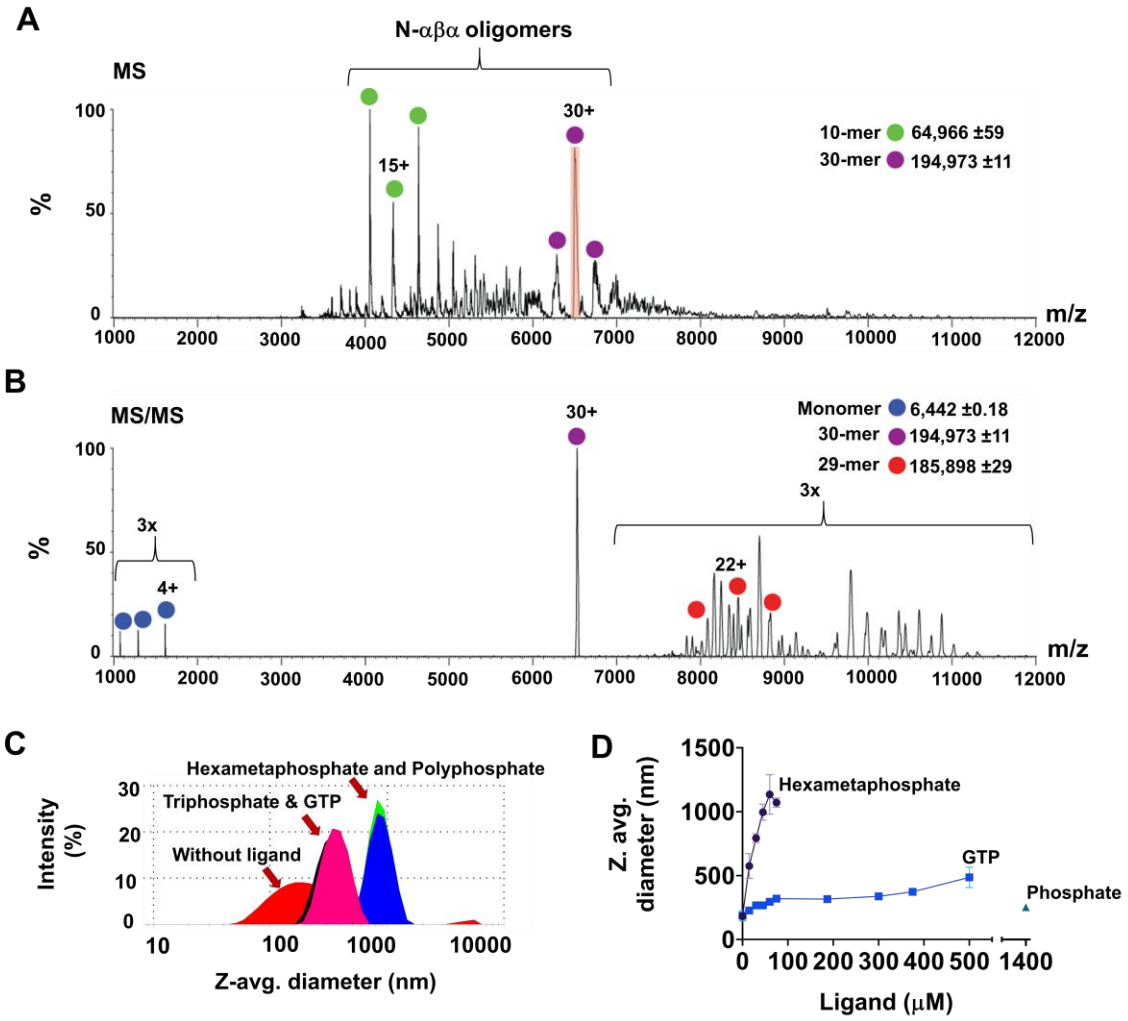

Figure 5. Quaternary structural characterization of N-αβα.

A. Native MS analysis of N-αβα prototype. Under non-dissociative conditions, charge series corresponding to 10 and 30 N-αβα oligomers were unambiguously assigned in the MS spectrum (green and purple dots, respectively). The 30+ charge state that was selected for tandem MS analysis is shadowed in red.

B. Tandem MS of the N-αβα 30-mer oligomer releases a highly charged monomer (blue; at the lower m/z range) and a stripped 29-mer oligomer (red), confirming the oligomer stoichiometry. The spectra are magnified 3-fold above 7,000 and below 2,000 *m/z*.

C. Dynamic light scattering (DLS) of N-αβα was monitored (1 μM protein, in 50 mM Tris buffer *plus* 100 mM NaCl, 25 °C), also upon addition of phosphoanyhidride ligands: hexametaphosphate and polyphosphate (both at 75 μM), or triphosphate and GTP (at 750

μM). Data were fit to the instrument's correlation function and analyzed by the method of cumulants [67] to obtain the z-average diameter (in nm).

D. The effect of phosphoanhydride ligands on the hydrodynamic particle size of N-αβα. Shown is the Z-avg. diameter as a function of ligand concentration. Vertical error bars represent standard deviation from three measurements.

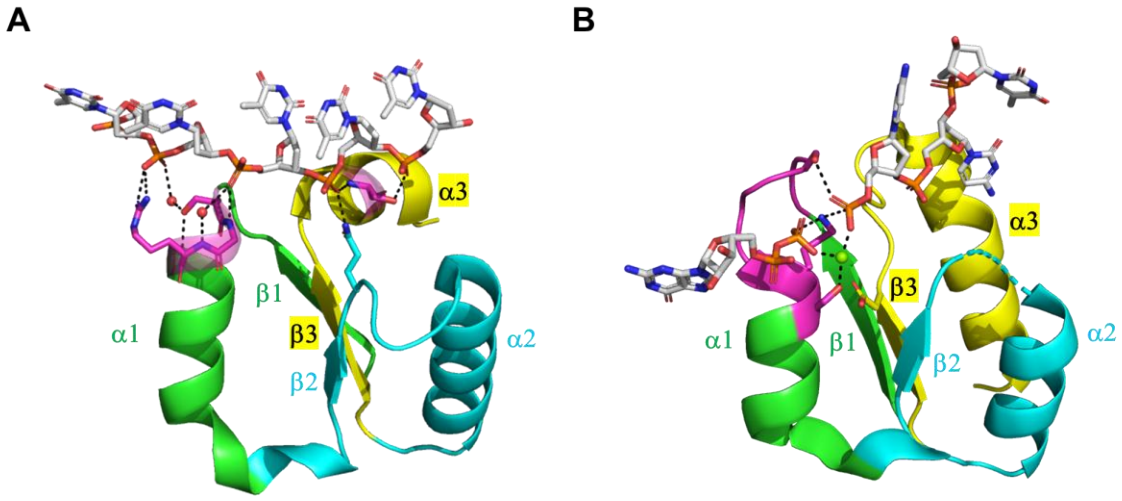

Figure 6: Instances of P-loops binding to ssDNA in extant P-loop NTPases.

A. The Helicase_C_2 domain of XPD helicases (F-groups, ECOD: 2004.1.1.106, Pfam: PF13307). Shown here is a fragment taken from a representative structure (ATP dependent DinG helicase; ECOD domain ID: e6fwrA1, residues 448-703; the fragment shown, residues 535-599, spans from β1 to α3). The strand topology of this domain follows the simplest P-loop NTPase topology (2-3-1-4-5). Its P-loop resides at the tip of α1, in the very same location as the Walker A, but its sequence is non-canonical (SGR, in magenta). Shown are direct as well as water-mediated interactions between the residues of the P-loop and phosphate groups of the ssDNA oligonucleotide (waters shown as red spheres). A glutamine at the tip of β2 (in cyan), and a serine at the N-terminus of α3 (in magenta) provide additional anchoring points for the ssDNA.

B. Bacterial polynucleotide kinase (F-groups, ECOD: 2004.1.1.32; Pfam: PF13671; strand topology: 2-3-1-4-5). Shown here is a fragment of the P-loop NTPase domain from a representative structure (*Clostridium thermocellum* polynucleotide kinase; ECOD domain ID: e4mdeA1, residues 1-170; the shown fragment, residues 8-37 and 62-98, spans from β1 to α3, with residues 38-61 truncated for clarity). The canonical Walker A motif resides between β1 and α1 (in magenta, GSSGSGKS) and binds GTP. This representative structure shows the product complex of GDP•Mg^{+2} and the phosphorylated ssDNA. The lysine and serine residues of the P-loop motif at the tip of α1 provide bridging interactions, coordinated by an Mg^{2+} ion (green sphere), between the β phosphate of the bound GDP and the phosphate group at the 5'-OH of the ssDNA.